Journal of Power Sources 183 (2008) 629–642

Contents lists available at ScienceDirect

Journal of Power Sources

journal homepage: www.elsevier.com/locate/jpowsour

Numerical investigation of the effect of cathode catalyst layer structure and composition on polymer electrolyte membrane fuel cell performance

Sai Kamarajugadda, Sandip Mazumder*

Department of Mechanical Engineering, The Ohio State University, Columbus, OH 43210, United States

ARTICLE INFO

Article history:
Received 30 April 2008
Received in revised form 20 May 2008
Accepted 21 May 2008
Available online 3 June 2008

Keywords:
Fuel cell
Polymer electrolyte membrane
Flooded agglomerate
Cathode catalyst layer
Modeling
Nafion loading
Platinum loading

ABSTRACT

The effect of the cathode catalyst layer's structure and composition on the overall performance of a polymer electrolyte membrane fuel cell (PEMFC) is investigated numerically. The starting point of the sub-grid scale catalyst layer model is the well-known flooded agglomerate concept. The proposed model addresses the effects of ionomer (Nafion) loading, catalyst (platinum) loading, platinum/carbon ratio, agglomerate size and cathode layer thickness. The sub-grid scale model is first validated against experimental data and previously published results, and then embedded within a two-dimensional validated computational fluid dynamics code that can predict the overall performance of the fuel cell. The integrated model is then used to explore a wide range of the compositional and structural parameter space, mentioned earlier. In each case, the model is able to correctly predict the trends observed by past experimental studies. It is found that the performance trends are often different at intermediate versus high current densities—the former being governed by agglomerate-scale (or local) losses, while the latter is governed by catalyst layer thickness-scale (or global) losses. The presence of an optimal performance with varying Nafion content in the cathode is more due to the local agglomerate-scale mass transport and conductivity losses in the polymer coating around the agglomerates than due to the amount of Nafion within the agglomerate. It is also found that platinum mass loading needs to be at a moderate level in order to optimize fuel cell performance, even if cost is to be disregarded.

1. Introduction

One of the impediments to commercial success of fuel cells is high cost. One of the major contributing factors to high cost is the excessive use of platinum within the catalyst layers. Thus, there is strong motivation for using as little platinum as possible without hampering the overall performance of the fuel cell. In a polymer electrolyte fuel cell (PEMFC), since the catalyst (typically platinum) is dispersed within a complex porous matrix comprised of carbon, the ionomer (typically Nafion) and platinum, the overall performance of the fuel cell does not scale linearly with an increase in the amount of platinum within the catalyst layer. Rather, the performance depends on how effectively the platinum is dispersed within the porous matrix so that most of it is actually utilized in catalyzing the electrochemical reactions. Since the proper functioning of a PEMFC cathode requires existence of triple phase boundaries [1,2] between the Nafion (for proton transfer), platinum (for catalysis) and carbon (for electron transfer), the determination of optimum composition and structure of the catalyst layer is a monumental task. Such studies are often undertaken using experiments [3,4], but are very time-consuming and expensive. Needless to say, with trial-and-error experimental procedures, only a small portion of the overall design space can be explored within a reasonable time. Computational modeling provides an alternative means to address this critical issue. However, such models also require careful formulation and, to some extent, calibration of unknown fitting parameters. Nevertheless, given the importance of the problem in the context of fuel cell technology advancement, and the difficulties associated with experimental trial-and-error procedures, there is strong motivation to try to address the problem using models, either fundamental or phenomenological.

Over the past decade or so, there has been an explosion in the number of technical publications that have reported findings of the simulation of the catalyst layer of a PEMFC. Broadly, these simulations may be classified into two categories: (1) simulations that utilize approximate models based on the pseudo-homogeneous film concept [5–9], or the flooded agglomerate concept [10–24], and (2) direct numerical simulation (DNS) of the catalyst layer [25,26]. While the latter approach is more powerful, it has serious limitations. First, it requires reconstruction of the catalyst layer

* Corresponding author at: Department of Mechanical Engineering, The Ohio State University, Suite E410, Scott Laboratory, 201 West 19th Avenue, Columbus, OH 43210, United States. Tel.: +1 614 247 8099; fax: +1 614 292 3163.
E-mail address: mazumder.2@osu.edu (S. Mazumder).

0378-7753/$ – see front matter © 2008 Elsevier B.V. All rights reserved.
doi:10.1016/j.jpowsour.2008.05.072

Nomenclature

A_v	total catalyst surface area per unit volume of cathode (m^{-1})
A_0	total catalyst surface area per unit mass of catalyst particle ($m^2\ kg^{-1}$)
c	dissolved oxygen concentration in Nafion ($kmol\ m^{-3}$)
c^*	dissolved oxygen concentration in Nafion in equilibrium with inlet gas ($kmol\ m^{-3}$)
$c_{O_2,g}$	oxygen gas concentration in cathode gas pores ($kmol\ m^{-3}$)
$c^*_{O_2,g}$	oxygen gas concentration at cathode inlet ($kmol\ m^{-3}$)
c_0^{ref}	standard reference oxygen concentration ($kmol\ m^{-3}$)
C_W	concentration of water in membrane ($kmol\ m^{-3}$)
$\bar{d}$	average pore size of cathode (m)
D_{kn}	binary diffusion coefficient of species k into n ($m^2\ s^{-1}$)
$D_{O_2,N}$	diffusion coefficient of oxygen in Nafion ($m^2\ s^{-1}$)
D_T	temperature dependence of D_λ ($m^2\ s^{-1}$)
D_W	diffusion coefficient of water ($m^2\ s^{-1}$)
D_λ	diffusion coefficient of water ($m^2\ s^{-1}$)
D'_λ	concentration dependence of D_λ
$D^{eff}_{O_2,N}$	effective diffusion coefficient of oxygen in Nafion in agglomerate ($m^2\ s^{-1}$)
Eff_1	nucleus effectiveness factor
Eff_2	film effectiveness factor
F	Faraday's constant ($96.487 \times 10^6\ C\ kmol^{-1}$)
$\mathbf{i}$	net current density vector ($A\ m^{-2}$)
$\mathbf{i}_F$	ionic phase current density vector ($A\ m^{-2}$)
$\mathbf{i}_S$	electronic phase current density vector ($A\ m^{-2}$)
i_s^{cat}	surface current density on a smooth catalyst surface ($A\ m^{-2}$)
i_0^{ref}	standard exchange current density on cathode ($A\ m^{-3}$)
j_0	reference current density ($A\ m^{-2}$)
j_T^{an}	net transfer current at anode due to electrochemical reaction ($A\ m^{-2}$)
j_T^{cat}	net transfer current density at cathode due to electrochemical reaction ($A\ m^{-3}$)
$\mathbf{J}_{adv}$	water flux due to advective transport ($kmol\ m^{-2}\ s^{-1}$)
$\mathbf{J}_{diff}$	water flux due to diffusion ($kmol\ m^{-2}\ s^{-1}$)
$\mathbf{J}_{drag}$	water flux due to electro-osmotic drag ($kmol\ m^{-2}\ s^{-1}$)
$\mathbf{J}_k$	diffusion mass flux of the kth species ($kg\ m^{-2}\ s^{-1}$)
L	cathode catalyst layer thickness (m)
m_{Pt}	platinum mass loading ($kg\ m^{-2}$)
M_m	molecular weight of the membrane ($kg\ kmol^{-1}$)
M_k	molecular weight of kth species ($kg\ kmol^{-1}$)
n	number of electrons transferred during the electrochemical reaction
$\hat{n}$	number of agglomerates per unit volume of cathode (m^{-3})
N	total number of gas-phase species
p	pressure (Pa)
Pt|C	platinum–carbon mass ratio in catalyst layer ink
r_{agg}	radius of agglomerate (m)
R	universal gas constant ($8314\ J\ kmol^{-1}\ K^{-1}$)
$\dot{S}_k$	production rate of kth species ($kg\ m^{-3}\ s^{-1}$)
$(S/V)_{eff}$	Effective surface to volume ratio (m^{-1})
t	time (s)
T	temperature (K)
$\mathbf{U}$	Bulk fluid velocity ($m\ s^{-1}$)
V_{oc}	open circuit voltage (V)
Y_k	mass fraction of kth species

Greek letters

α_a,α_c	Tafel constants for anode
α_T	Tafel constant for cathode catalyst model
β_k	concentration exponents for the kth species
δ	polymer coating thickness around agglomerate nucleus (m)
ε	wet porosity
ε_{agg}	volume fraction of polymer in agglomerate nucleus
ε_{cat}	porosity of cathode catalyst layer
ε_S	volume fraction of platinum + carbon in cathode
ε_N	volume fraction of polymer in cathode
η	electrode overpotential (V)
η_d	electro-osmotic drag coefficient
κ	permeability (m^2)
λ	water content
$[\Lambda_k]$	molar concentration of species k ($kmol\ m^{-3}$)
μ	dynamic viscosity ($kg\ m^{-1}\ s^{-1}$)
ρ	mass density of mixture ($kg\ m^{-3}$)
ρ_C	density of carbon ($kg\ m^{-3}$)
ρ_{Pt}	density of platinum ($kg\ m^{-3}$)
ρ_m^{dry}	density of dry membrane ($kg\ m^{-3}$)
σ	electrical conductivity ($\Omega^{-1}\ m^{-1}$)
σ_F	electrical conductivity of the ionic phase ($\Omega^{-1}\ m^{-1}$)
σ_S	electrical conductivity of the electronic phase ($\Omega^{-1}\ m^{-1}$)
σ_{30}	concentration dependence of electrical conductivity ($\Omega^{-1}\ m^{-1}$)
τ_{cat}	tortuosity of cathode
Φ_F	ionic phase potential (V)
Φ_S	electronic phase potential (V)

microstructure from SEM or TEM images. Secondly, direct numerical simulations are difficult to perform and are very expensive. Simulation times for a single case may often run into days. Finally, certain compromises have to be made with regard to the actual geometry [25], rendering the results of these studies inconclusive in many cases. Nevertheless, this approach is often useful for fundamental understanding of the coupling between transport phenomena and heterogeneous reactions at the micro-scale and can be used as a framework to develop simplified models.

The more popular approach is based on models of coupled transport and reactions within the catalyst layer structure. Historically, two different model types have been used for this purpose. The first model type, generally referred to in the literature as the pseudo-homogeneous film model [5–9], assumes that the catalyst layer is a porous matrix comprised of Nafion, platinum, and carbon in random (homogeneous) configuration. This model allows for pathways of gases, electrons, and protons within the catalyst layer, and captures some of the essential transport phenomena prevalent in the catalyst layer. However, this model does not acknowledge the necessity for the existence of the triple-phase boundary for a functioning catalyst layer. In contrast, the flooded agglomerate concept, proposed in the late 1980s [10,11], contends that the platinum is supported on carbon particles, which forms agglomerates when mixed with an ionomer. The agglomerate may even be coated fully

or partially by an additional ionomer layer. The oxygen finds its way to the platinum by first dissolving in the ionomer, and is consumed as it transports to the core of the carbon–platinum aggregate. From the preceding discussion, it is clear that this model guarantees the existence of triple-phase boundaries as long as sufficient amounts of the ionomer are present. Microscopic observations [13,20] support the structure proposed by this model, and recent calculations performed using this model appear to match experimental data better than the pseudo-homogeneous film model [8,19]. It is worth noting that the popularity of the flooded agglomerate model is in part due to the fact that modeling studies using this model have also shown that the choice of spherical or cylindrical agglomerates did not significantly alter the overall performance of the PEMFC [27], indicating that the exact geometrical shape of the agglomerate is, perhaps, not of great importance. This finding presents another reason not to pursue tedious DNS studies.

Most notable among recent studies that have used the flooded agglomerate model is the work of Jaouen et al. [15,16,27], Sun et al. [18], and Secanell et al. [19]. Jaouen et al. have successfully used this model to predict the performance of the cathode as a function of operating conditions and cathode layer thicknesses. Their calculations predicted experimentally observed double Tafel slopes [16], attributed to local (within agglomerate) mass transport limitations. However, the model was not exercised to study effect of other compositional variables such as Nafion loading and platinum loading. Such studies were performed by Sun et al. [18], who predicted an optimum Nafion loading—consistent with experimentally observed behavior [3,4]. Studies performed by both Sun et al. [18] and Secanell et al. [19] suggests that the performance of the cathode improves monotonically as the agglomerate radius is decreased. However, it is believed [27] that excessive reduction in the agglomerate radius can lead to severe reduction in the size of the macropores and high tortuosity. This, in turn, can result in deterioration of the performance, especially at high current densities, due to global mass transport limitations.

In this study, we generalize the flooded agglomerate model by carefully assimilating findings of past studies, and extending the core model to include the following effects: (1) effect of Nafion loading, (2) effect of catalyst (platinum) loading, (3) effect of carbon–platinum ratio, (4) agglomerate radius, and (5) cathode catalyst layer thickness. In an effort to do so, care has been exercised to account for both local (agglomerate-scale) as well as global (catalyst layer thickness-scale) effects. Whenever possible, an attempt has also been made to compare predicted results with experimental findings, at least qualitatively.

2. Model description

2.1. Agglomerate model

In our agglomerate model, the cathode is assumed to be comprised of a large number of spherical agglomerates surrounded by gas pores (Fig. 1). An agglomerate, in turn, is comprised of clusters of carbon supporting platinum particles held together by proton-conducting polymer. The agglomerate may be coated with a thin film of polymer (Fig. 2). Thus, the cathode consists of three components: the solid carbon–platinum clusters, the polymer electrolyte, and gas pores. For the model to be valid, the agglomerate size must be sufficiently small compared to the cathode layer thickness such that the potential within an agglomerate may be assumed to be constant. Transport of reactants from the cathode channel to the cathode active layer is dominated by diffusion within the pores of the cathode diffusion layer and the cathode catalyst layer (see Fig. 1). Oxygen reaches platinum within the agglomerate by dissolution into the polymer coating followed by diffusion through the polymer within the agglomerate. The purpose of the sub-grid scale agglomerate model is to provide a means to calculate the volumetric current density ($A\,m^{-3}$) in the cathode catalyst layer. Expressions to this effect are derived in this section. Expressions for volume fractions of the three components of the cathode, which influence various effective transport properties, are also derived in this section.

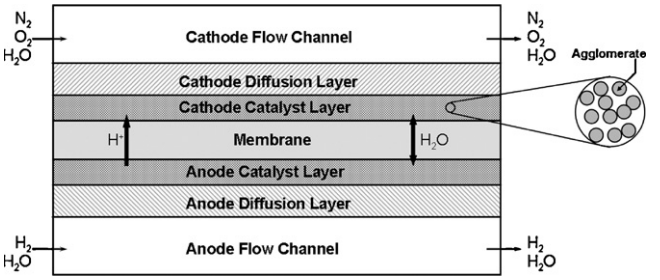

Fig. 1. Schematic representation of a cross-section of a PEM fuel cell. The magnified portion of the cathode catalyst layer shows a representation of the uniformly distributed spherical agglomerates surrounded by gas pores.

The oxygen reduction reaction (ORR) kinetics in the polymer electrolyte is assumed to follow a Tafel law and to be first-order in oxygen concentration. Hence, the surface current density on a smooth catalyst surface is given by [15]:

$$i_s^{cat} = -i_0^{ref}\left(\frac{c^*}{c_{O_2}^{ref}}\right)^{1-\alpha_T/n} \exp\left(-\frac{\alpha_T F}{RT}\eta\right)\frac{c}{c^*} \tag{1}$$

where $c_{O_2}^{ref}$ is the standard reference oxygen concentration, i_0^{ref} is the standard exchange current density for a smooth catalyst surface, and η is the local overpotential defined as the difference between the electronic and protonic phase potentials, *i.e.*, $\eta = \phi_s - \phi_F$. c and c^* are the dissolved oxygen concentration in the polymer at the catalyst surface and the dissolved oxygen concentration in the polymer in equilibrium with the inlet gas, respectively.

Within the agglomerate, oxygen is assumed to diffuse through the polymer electrolyte to the catalyst surface according to Fick's law. While it diffuses through the agglomerate, it reacts on the platinum clusters impregnated on the carbon surfaces, and is consumed (Fig. 2). This phenomenon is best described by the following reaction-diffusion balance equation [15]:

$$D_{O_2,N}^{eff}\left(\frac{d^2c}{dr^2} + \frac{2}{r}\frac{dc}{dr}\right) + \gamma\frac{A_v i_s^{cat}(1-\varepsilon_{agg})}{nF} = 0$$

$$\gamma = 1 \text{ for } 0 \le r \le r_{agg};\ \gamma = 0 \text{ for } r_{agg} \le r \le (r_{agg}+\delta) \tag{2}$$

The boundary conditions for the above equation are as follows [15]:

$$\left.\frac{dc}{dr}\right|_{r=0} = 0 \tag{3a}$$

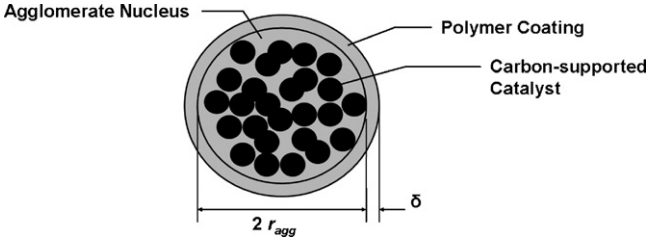

Fig. 2. Agglomerate nucleus with carbon-supported catalyst particles distributed in polymer with a polymer coating around the nucleus.

$$c(r_{agg}^{-}) = c(r_{agg}^{+}) \tag{3b}$$

$$D_{O_2,N}^{eff} \left.\frac{dc}{dr}\right|_{r=r_{agg}^{-}} = D_{O_2,N} \left.\frac{dc}{dr}\right|_{r=r_{agg}^{+}} \tag{3c}$$

$$c(r_{agg}+\delta) = \frac{c^*}{c_{O_2,g}^*} c_{O_2,g} = H c_{O_2,g} \tag{3d}$$

where r_{agg} is the radius of the agglomerate nucleus, δ is the thickness of the polymer coating around the agglomerate, ε_{agg} is the volume fraction of polymer present within the agglomerate nucleus, and A_v is the total catalyst surface area per unit volume. Eq. (3d) represents equilibrium between dissolved oxygen concentration in Nafion (c) and oxygen concentration in the gas pores ($c_{O_2,g}$) at the outer surface of the polymer coating, where H is Henry's constant. The term $c_{O_2,g}^*$ in Eq. (3d) represents the concentration of oxygen at cathode inlet. $D_{O_2,N}^{eff}$ is the effective oxygen diffusion coefficient in Nafion within the agglomerate, and is obtained from the Bruggemann relation as [28]:

$$\begin{aligned} D_{O_2,N}^{eff} &= D_{O_2,N}\varepsilon_{agg}^{1.5} \quad \text{for } r \le r_{agg} \\ D_{O_2,N}^{eff} &= D_{O_2,N} \quad \text{for } r_{agg} \le r \le (r_{agg}+\delta) \end{aligned} \tag{4}$$

The system of equations, Eqs. (1)–(3), can be solved analytically. It yields an expression for the volumetric current density in the cathode, written as [15]:

$$j_T^{cat} = -A_v(1-\varepsilon_{agg}) i_0^{ref} \left(\frac{c^*}{c_{O_2}^{ref}}\right)^{1-\alpha_T/n} \times \exp\left(-\frac{\alpha_T F}{RT}\eta\right) \mathrm{Eff}_1\, \mathrm{Eff}_2 (1-\varepsilon_{cat}) \frac{r_{agg}^3}{(r_{agg}+\delta)^3} \frac{c_{O_2,g}}{c_{O_2,g}^*} \tag{5}$$

where ε_{cat} is the porosity of the cathode catalyst layer, $c_{O_2,g}$ and $c_{O_2,g}^*$ are the oxygen concentrations at the polymer-coating–gas-pore interface and at the inlet, respectively. Eff_1 and Eff_2 are the nucleus and film effectiveness factors. They represent corrections to the pure kinetic current density due to diffusion limitations in the agglomerate nucleus and the polymer coating, respectively. Eff_1 and Eff_2 are written as follows [15]:

$$\mathrm{Eff}_1 = \frac{3}{q r_{agg}} \left(\frac{1}{\tanh(q r_{agg})} - \frac{1}{q r_{agg}}\right) \tag{6}$$

$$\mathrm{Eff}_2 = \frac{1}{1+(1/3)(r_{agg}^2\delta)/(r_{agg}+\delta) q^2 \varepsilon_{agg}^{1.5} \mathrm{Eff}_1} \tag{7}$$

where

$$q^2 = \frac{A_v(1-\varepsilon_{agg}) i_0^{ref} \left(c^*/c_{O_2}^{ref}\right)^{1-\alpha_T/n} \exp\left(-(\alpha_T F)/(RT)\eta\right)}{n F D_{O_2,N} c^* \varepsilon_{agg}^{1.5}} \tag{8}$$

Since Eff_1 and Eff_2 represent corrections to the pure kinetic current density, it is informative to investigate how they change with r_{agg}, ε_{agg} and δ in order to gain an understanding of how the agglomerate-level mass transport losses behave. Fig. 3 shows a plot of these two quantities. It is seen from Fig. 3(a)–(c) that the local mass transport losses are largest (Eff_1 is smallest) when the agglomerate radius, r_{agg}, is large and the Nafion volume fraction within the agglomerate, ε_{agg}, is small. And the losses are larger at larger values of the cathode overpotential. It is also observed that the film coating has almost no effect on local mass-transport losses, probably because the film coating thickness is small in the first place.

The parameter A_v represents the total catalyst surface area per unit volume of cathode catalyst layer available for the ORR. This value is related to the platinum mass loading (m_{Pt}), the platinum particle size and the platinum to carbon mass ratio (Pt|C) in the catalyst layer ink. The dependence of this parameter on the platinum mass loading is given as [19]:

$$A_v = A_0 \frac{m_{Pt}}{L} \tag{9}$$

where A_0 is the total catalyst surface area per unit mass of catalyst particle. Based on empirical data provided by Marr and Li [6] for various platinum supported catalysts, Secanell et al. [19] estimated this value using the following correlation:

$$\begin{aligned} A_0 = {} & 2.2779\times10^6(\mathrm{Pt|C})^3 - 1.5857\times10^6(\mathrm{Pt|C})^2 \\ & -2.0153\times10^6(\mathrm{Pt|C}) + 1.5950\times10^6 \end{aligned} \tag{10}$$

In order to compute the effective properties for transport in the cathode catalyst layer, the volume fractions of the three components of the cathode, namely the solid component comprised of carbon–platinum clusters, the proton-conducting polymer component and the porous component for mass transport, need to be calculated. The composition of the catalyst layer ink used strongly influences these volume fractions.

The solid component volume fraction is given by the amounts of platinum and carbon in the cathode layer. These values are obtained from the platinum mass loading (m_{Pt}) and the platinum to carbon mass ratio (Pt|C) in the catalyst layer ink. The solid component volume fraction is obtained as [19]:

$$\varepsilon_S = \left(\frac{1}{\rho_{Pt}} + \frac{1-\mathrm{Pt|C}}{\mathrm{Pt|C}\rho_C}\right) \frac{m_{Pt}}{L} \tag{11}$$

where ρ_{Pt} and ρ_C are the densities of platinum and carbon respectively, and L is the cathode catalyst layer thickness.

Under the assumption that the cathode catalyst layer consists of spherical agglomerates, and that the agglomerates are made up of only the solid component and the polymer, the number of agglomerates per unit volume required to obtain the above solid component volume fraction is given by the following equation [19]:

$$\hat{n} = \frac{\varepsilon_S}{(4/3)\pi r_{agg}^3 (1-\varepsilon_{agg})} \tag{12}$$

Assuming that the entire polymer electrolyte in the cathode catalyst layer is only present either in the agglomerate nucleus or in the polymer coating around the agglomerate, the volume fraction of the polymer in the cathode can be obtained from [19]:

$$\varepsilon_N = \frac{4}{3}\pi\hat{n}\left[r_{agg}^3\varepsilon_{agg} + \left\{(r_{agg}+\delta)^3 - r_{agg}^3\right\}\right] \tag{13}$$

where δ is the average thickness of the polymer film coating around the agglomerate.

Once the volume fractions of the solid component and the polymer are obtained, the porosity of the cathode catalyst layer is obtained as

$$\varepsilon_{cat} = 1 - \varepsilon_S - \varepsilon_N \tag{14}$$

This volume fraction represents the volume of macro-pores in the cathode catalyst layer which is available for transport of reactants.

As can be seen from Eqs. (1), (2), (3a)–(3d), (4)–(14), the transport properties, as well as the parameters for electrochemical reaction kinetics are simultaneously influenced by the radius of agglomerate nucleus (r_{agg}), the agglomerate coating thickness (δ), volume fraction of polymer within the agglomerate nucleus (ε_{agg}), platinum mass loading (m_{Pt}), platinum–carbon mass ratioin the

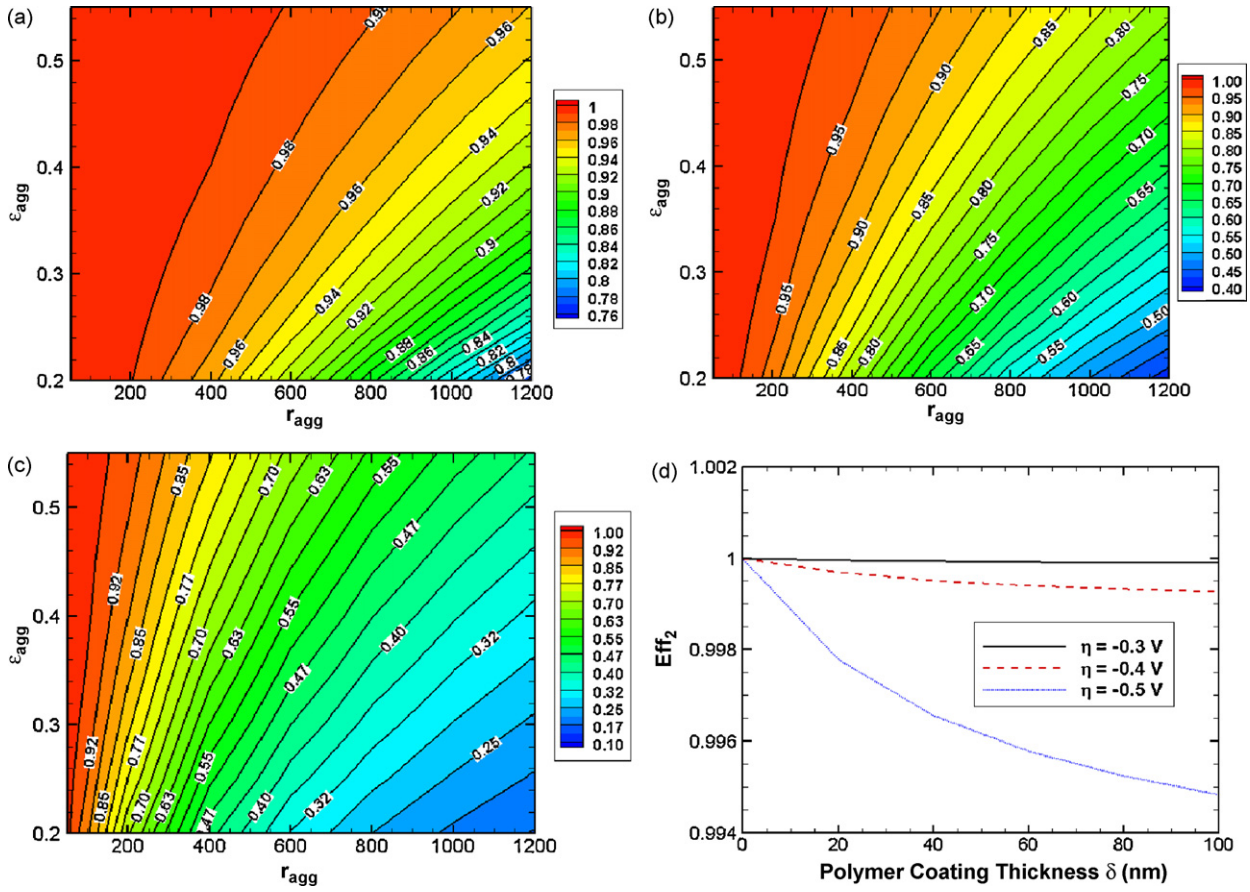

Fig. 3. Nucleus effectiveness factor (Eff_1) with varying agglomerate radius and polymer volumetric fraction within agglomerate nucleus for nominal cathode overpotential values of (a) $\eta_{cat} = -0.3$ V, (b) $\eta_{cat} = -0.4$ V, and (c) $\eta_{cat} = -0.5$ V. Using the maximum value of the nucleus effectiveness factor, the effect of the polymer coating thickness (δ) on the film effectiveness factor (Eff_2) is presented in (d). Kinetic constants for these calculations were obtained using $L = 15$ μm, $m_{Pt} = 0.4$ mg cm^{-2} and Pt|C = 0.28.

catalyst layer ink (Pt|C), and the cathode catalyst layer thickness (L).

2.2. Computational fluid dynamics (CFD) model

The sub-grid scale catalyst layer model, described in the preceding section, was implemented into a two-dimensional computational fluid dynamics (CFD) code that has been developed specifically for PEMFC applications, and has been validated [29]. The purpose of this step is to enable prediction of the overall performance (polarization behavior) of the fuel cell by taking into account both local and global losses. The governing equations are the equations of conservation of mass (both overall and individual species), momentum, energy, and charge. For simplicity, it is assumed that the temperature does not change spatially, and thus, the energy conservation equation is not solved. Furthermore, it is assumed that water exists only in its vapor phase in gas diffusion layers and channels, and two-phase effects are not considered. The governing conservation equations are different inside and outside the membrane and are, therefore, presented here separately.

2.2.1. Channels, gas diffusion layers (GDL), and active catalyst layers (ACL)

The governing conservation equations for mass and momentum, are written as [30–32]:

$$\text{overall mass}: \frac{\partial}{\partial t}(\varepsilon\rho) + \nabla\cdot(\varepsilon\rho\mathbf{U}) = \dot{S}_m \tag{15}$$

$$\text{momentum}: \frac{\partial}{\partial t}(\rho\varepsilon\mathbf{U}) + \nabla\cdot(\rho\varepsilon\mathbf{U}\mathbf{U}) = -\varepsilon\nabla p + \nabla\cdot(\mu_{eff}\nabla\mathbf{U}) + \frac{\mu\varepsilon^2\mathbf{U}}{\kappa} \tag{16}$$

$$\text{species mass}: \frac{\partial}{\partial t}(\rho Y_k) + \nabla\cdot(\rho\mathbf{U}Y_k) = -\nabla\cdot\mathbf{J}_k + \dot{S}_k \quad \forall k = 1, 2, \ldots, N \tag{17}$$

where ρ is the density, p is the pressure, μ is the dynamic viscosity of the fluid, and $\mathbf{U}$ is the fluid velocity vector. ε is the porosity of the medium and κ is the permeability. In Eq. (15), $\dot{S}_m$ is the mass source term due to electrochemical reactions, and is non-zero only in the catalyst layers. It results from the fact that a conservation equation for protons is not directly solved, and therefore, the mass of protons created or destroyed need to be subtracted out of the overall continuity equation. The last term in Eq. (16) represents the sub-grid scale drag force imposed by the pore walls on the fluid, written using the linear Darcy's Law [28]. In purely open regions, such as in the gas channels, $\varepsilon \to 1$ and $\kappa \to \infty$, and Eqs. (15) and (16) reduce to the well-known Navier–Stokes equations. In Eq. (17), Y_k is the mass fraction of the kth species, $\mathbf{J}_k$ is the mass diffusion flux of the kth species, and $\dot{S}_k$ is the production rate of the kth species due to electrochemical reactions. The total number of species in the system is denoted by N.

The diffusion flux of the kth species, $\mathbf{J}_k$, is modeled using the so-called dilute approximation [33]. By this approximation, the

diffusion flux is written as

$$\mathbf{J}_k = -\rho D_{km} \nabla Y_k \tag{18}$$

where D_{km} is the free-stream diffusivity of species k into the mixture, and is henceforth denoted by D_k for simplicity. The free-stream diffusivity is given by the following relation [33]:

$$D_{km} = D_k = \frac{1 - X_k}{\sum_{i=1, i\neq k}^{N} \frac{X_i}{D_{ki}}} \tag{19}$$

where D_{ki} is the binary diffusivity of species k into species i, and X_k is the mole fraction of the kth species. Substitution of Eq. (18) into Eq. (17) yields the appropriate species transport equation under the dilute approximation formulation for open regions:

$$\frac{\partial}{\partial t}(\varepsilon \rho Y_k) + \nabla \cdot (\varepsilon \rho U Y_k) = \nabla \cdot (\rho D_k \nabla Y_k) + \dot{S}_k \quad \forall k = 1, 2, \ldots, N \tag{20}$$

In porous regions, it is customary to use the so-called Bruggemann relation [28], and modify the free-stream diffusion coefficient, such that the governing species conservation equation becomes

$$\frac{\partial}{\partial t}(\varepsilon \rho Y_k) + \nabla \cdot (\varepsilon \rho \mathbf{U} Y_k) = \nabla \cdot \left(\rho D_k \varepsilon^{\tau} \nabla Y_k\right) + \dot{S}_k \quad \forall k = 1, 2, \ldots, N \tag{21}$$

where τ is the tortuosity of the porous region. Traditionally, a value of $\tau = 15$ is used in Eq. (21). In order to examine the effect of cathode structure and tortuosity on fuel cell performance, a more sophisticated tortuosity model, proposed by Abbasi et al. [34], is used. Hence the governing species conservation equation in the cathode catalyst layer becomes:

$$\frac{\partial}{\partial t}(\varepsilon_{cat} \rho Y_k) + \nabla \cdot (\varepsilon \mathrm{cat}_{\rho} \mathbf{U} Y_k) = \nabla \cdot \left(\rho D_k \frac{\varepsilon_{cat}}{\tau_{cat}} \nabla Y_k\right) + \dot{S}_k \quad \forall k = 1, 2, \ldots, N \tag{22}$$

where the tortousity τ_{cat} is given by [34]:

$$\tau_{cat} = \frac{1}{\varepsilon_{cat}} + 1.196 \frac{\sigma_{dev}}{\bar{d}} \tag{23}$$

where σ_{dev} is the standard deviation of the pore size in the cathode catalyst layer. In this study, a constant value of $\sigma_{dev} = 50$ nm has been used for the sake of convenience. $\bar{d}$ is the average pore size of the cathode catalyst layer, and is given by [35]:

$$\bar{d} = \frac{4}{3} \frac{\varepsilon_{cat}}{(1 - \varepsilon_{cat})} r_{agg} \tag{24}$$

Clearly, this tortuosity model explicitly accounts for the agglomerate radius variation in addition to variations in the global porosity (as stipulated by the Bruggemann model). Thus, one can account for changes in tortuosity (and mass transport resistance) due to change in the agglomerate size while keeping the overall porosity unchanged—an effect that cannot be predicted by the Bruggemann model. The differences between the diffusion coefficients predicted by the two models are shown in Fig. 4. The key observation from this figure is that for a constant porosity, the Bruggemann model does not predict any variation of the diffusion coefficient with agglomerate (or pore) size, while the model used here predicts a sharp drop in the effective diffusion coefficient when the agglomerate (or pore) size becomes significantly small.

The source due to the electrochemical reactions is non-zero only in the active catalyst layers of the anode and cathode, and is zero elsewhere. It is written as [36]:

$$\dot{S}_k = \frac{j_T M_k}{2nF} \left(\frac{S}{V}\right)_{eff} \tag{25}$$

where j_T is the net transfer current due to electrochemical reaction, M_k is the molecular weight of the kth species, n is the number

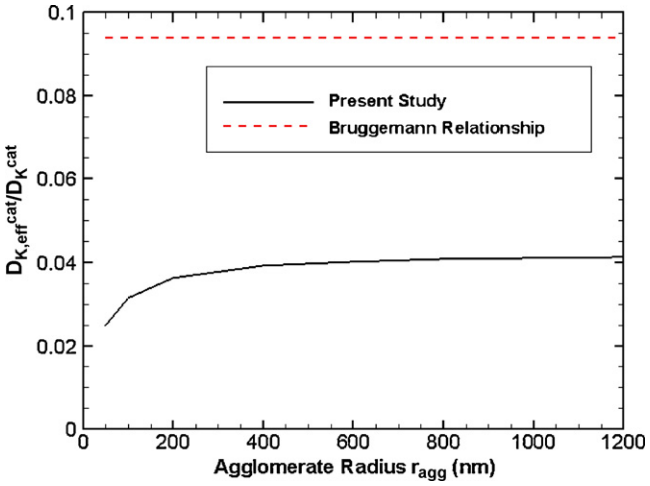

Fig. 4. Effect of agglomerate radius (r_{agg}) on non-dimensional effective gas diffusivities in cathode for $L = 15$ μm, $\delta/r_{agg} = 0.06$, $\varepsilon_{agg} = 0.4$, $m_{Pt} = 0.45$ mg cm^{-2} and Pt|C = 0.28. In the figure, $D_{k,eff}^{cat}$ stands for the effective diffusivity of species k into the gas mixture in the cathode catalyst layer, while D_k^{cat} stands for the free stream diffusivity of species k into the gas mixture in the cathode catalyst layer.

of electrons transferred during the electrochemical reaction, and F is the Faraday constant. $(S/V)_{eff}$ represents the ratio of the active surface area of the catalyst to its overall volume (including the support). The anode transfer current j_T^{an} is expressed using the Butler–Volmer equation [36]:

$$j_T^{an} = j_0 \left[\exp\left(\frac{\alpha_a F}{RT}\eta\right) - \exp\left(-\frac{\alpha_c F}{RT}\eta\right)\right] \prod_{k=1}^{N} [\Lambda_k]^{\beta_k} \tag{26}$$

where j_0 is the reference current density, α_a and α_c are kinetic constants determined from experimentally measured Tafel plots. $[\Lambda_k]$ and β_k are the molar concentrations and the concentration exponents for the kth species, respectively. η is the electrode overpotential (including both activation and concentration overpotential) and is defined as the difference between the electronic or solid phase potential (ϕ_S) and the electrolyte or ionic phase potential (ϕ_F), *i.e.*, $\eta = \phi_S - \phi_F$. In this study, the above Butler–Volmer kinetic relation was used only for the anode, while the cathode transfer current was obtained from Eq. (5) (Section 2.1).

In a PEMFC calculation, in addition to mass conservation, it is necessary to enforce charge conservation. Under the assumption of electro-neutrality, charge conservation reduces to current conservation, written as

$$\nabla \cdot \mathbf{i} = 0 \tag{27}$$

where $\mathbf{i}$ is the current density vector. In a PEMFC, the current flow is due to protons (H^+) flowing through the membrane, resulting in an ionic phase current ($\mathbf{i}_F$), and due to electrons flowing through the carbon in the porous matrix of the gas diffusion layers, resulting in an electronic phase current ($\mathbf{i}_S$). Thus, Eq. (27) can be rewritten as follows:

$$\nabla \cdot \mathbf{i}_F + \nabla \cdot \mathbf{i}_S = 0 \tag{28}$$

Since current transport in the ionic phase is due to ions and that in the electronic phase is due to electrons, the transport in each phase is governed by separate electric potential fields. Using Ohm's law, Eq. (28) can be written as

$$\nabla \cdot (\sigma_F \nabla \phi_F) + \nabla \cdot (\sigma_S \nabla \phi_S) = 0 \tag{29}$$

where σ_F and σ_S are the conductivities of the ionic and electronic phases, respectively. The exchange of current from the ionic to the

electronic phase occurs due to electrochemical reactions during which electrons are transferred from one phase to the other. Thus, Eq. (29) can be rewritten as [31,36]:

$$-\nabla\cdot(\sigma_F\nabla\phi_F)=\nabla\cdot(\sigma_S\nabla\phi_S)=j_T\left(\frac{S}{V}\right)_{\text{eff}} \tag{30}$$

Eq. (30) represents two elliptic partial differential equations that are strongly coupled through the transfer current source. The ionic phase electric potential equation (for ϕ_F) must be solved in the ACL and the membrane, while the electronic phase electric potential equation (for ϕ_S) must be solved in the ACL and the GDL (see Fig. 1). In the ACL, both equations are solved, and are strongly coupled. The difference in value between ϕ_S and ϕ_F represents the total electrode overpotential.

2.2.2. Water and current transport in membrane

Nafion membranes are, for all practical purposes, impermeable to all gases except water. Thus, the governing equation for species transport outside the membrane (Eq. (17)) is irrelevant in this context. The only species that needs to be considered is water. For all other species, zero flux boundary conditions must be used at the membrane-ACL interface. Water transport in the membrane of a PEMFC occurs primarily due to diffusion and electro-osmotic drag, although there is some evidence that pressure-driven advection may also occur [37–41]. In phenomenological membrane models, it is customary to express water transport in terms of the water content, λ, as [42]:

$$\nabla^{\circ}\left[\eta_d\frac{\mathbf{i}}{F}\right]=\nabla^{\circ}\left[\frac{\rho_m}{M_m}D_\lambda\nabla\lambda\right] \tag{31}$$

The water content is defined as the ratio of the number of water molecules to the number of $SO_3^-H^+$ charge sites in the medium. In Eq. (31), it has been assumed that advective transport is negligible. D_λ denotes the diffusion coefficient of water in Nafion expressed in terms of the water content, η_d denotes the electro-osmotic drag coefficient, and ρ_m/M_m represents the molar density of the membrane. Fuller and Newman [43] give the diffusion coefficient as:

$$D_\lambda=(2.1\times10^{-7})\times\lambda\times\exp\left[-\frac{2436}{T}\right] \tag{32}$$

The electro-osmotic drag coefficient is given by [44]:

$$\eta_d=\frac{2.5}{22}\lambda \tag{33}$$

Current transport in the membrane is described by the ionic phase part of Eq. (30), except that there is no source, *i.e.*, the right hand side of the equation is zero. The ionic phase electrical conductivity of the membrane, σ_F, is again expressed by the empirical correlation [44]:

$$\sigma_F=100\exp\left[1268\left(\frac{1}{303}-\frac{1}{T}\right)\right]\sigma_{30} \tag{34}$$

where σ_{30} is the electrical conductivity of the membrane at 30 °C, and is given by [43]:

$$\sigma_{30}=0.005139\lambda-0.00326\quad\text{for}\ \lambda>1 \tag{35}$$

The ionic phase electrical conductivities in the anode catalyst layer and the cathode catalyst layer are evaluated using Eqs. (34) and (35) based on local values of water content. However, in these regions, the conductivities need to be corrected in order to account for the fact that the proton-conducting polymer is just one of the components in the layer. The effective ionic phase electrical conductivity in the cathode is given by Jaouen et al. [15] as:

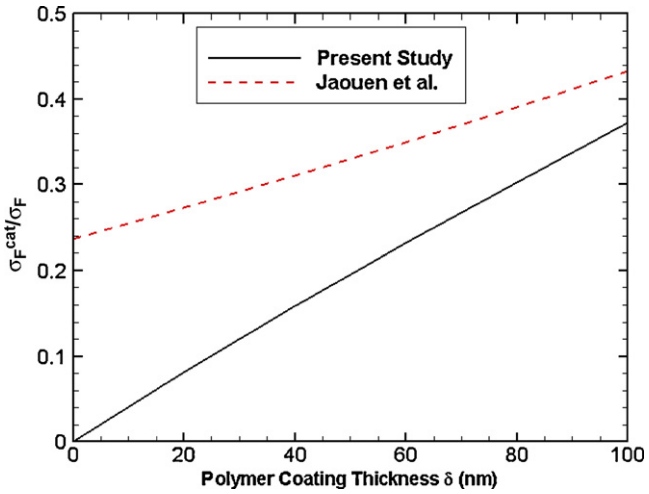

Fig. 5. Effect of polymer coating thickness (δ) on non-dimensional effective protonic conductivity of cathode for $L=15\,\mu m$, $r_{agg}=1000\,nm$, $\varepsilon_{agg}=0.4$, $m_{Pt}=0.4\,mg\,cm^{-2}$ and Pt|C = 0.28.

$$\sigma_F^{cat}=(1-\varepsilon_{cat})\left[1+\frac{(\varepsilon_{agg}-1)}{(1+\delta/r_{agg})^3}\right]\sigma_F \tag{36}$$

Proton transport between agglomerates requires that there be sufficient polymer coating around agglomerates. As the coating thickness decreases, the contact between agglomerates decreases, which in turn leads to decreased proton transport. To better capture this trend, we need that as $\delta\to0$, $\sigma_F^{cat}\to0$ as well. To this end, in the present model, the effective ionic phase electrical conductivity in the cathode is modified to

$$\sigma_F^{cat}=(1-\varepsilon_{cat})\left[1+\frac{(\varepsilon_{agg}-1)}{(1+\delta/r_{agg}+a_o)^3}\right]\sigma_F \tag{37}$$

where a_o is given by:

$$a_o=\min\left[0,\left(\frac{\delta}{r_{agg}}+(1-\varepsilon_{agg})^{1/3}-1\right)\right] \tag{38}$$

Eq. (37) satisfies the requirement that very low values of δ lead to very low values of σ_F^{cat}, while returning the values obtained from Eq. (36) at sufficiently high values of δ, as shown in Fig. 5. It is worth noting that the contention that the agglomerate is coated with a uniformly thick layer of the ionomer is an assumption in the flooded agglomerate model. Clearly, that would make it impossible for electrons to flow from one carbon particle to another. However, in a real 3D microstructure, there is always some partial contact between the cores of adjacent agglomerates, which makes electron transport possible.

It is evident from Eqs. (31)–(35) that the two quantities that dictate the mass transport and electrical properties of a Nafion membrane are its water content and temperature. The water content is obtained by solution of the conservation equation for water (Eq. (31)). However, solution of this equation requires specification of either the water content itself or the flux of water at the membrane–ACL interface, which in turn requires coupling with the rest of the computational domain. Various approaches for coupling the membrane with the overall calculation procedure and for implementation of the interface conditions are discussed in Kamarajugadda and Mazumder [29].

3. Results and discussion

The governing conservation equations of mass, momentum and current, described in the preceding section, were solved using a conservative finite-volume technique [45]. The SIMPLE algorithm [45] was used to address pressure–velocity coupling in the Navier–Stokes equations. The 2D model, shown in Fig. 1, was used for simulations. All simulations were performed on a uniform grid with 50 cells in the axial direction and 150 cells in the cross-flow (y) direction. Nominally, 40 cells were used across each flow channel, 10 across each GDL, 5 across each active catalyst layer, and 40 across the membrane. This particular mesh size was chosen after a rigorous grid-independence study, the details of which can be found in Kamarajugadda and Mazumder [29].

Moist hydrogen and moist air was introduced into the anode and cathode inlet, respectively. A plug velocity profile was imposed, and the magnitude of the velocity was calculated from a prescribed equivalent current density. For all simulations, the temperature was assumed to be 50 °C everywhere, and the energy equation was not solved. Other relevant parameters used for simulations are reported in Table 1. The kinetic constant, j_0, for the electrochemical reactions at the anode was determined by calibrating the current density at low bias voltage against experimental data reported by Ticianelli et al. [46,47]—a practice that has been used in the past [31]. All simulations were run with a prescribed bias voltage boundary condition rather than a prescribed current boundary condition.

All transport properties of the fluid, namely viscosity and binary diffusion coefficients were computed using the Chapman–Enskog equations of kinetic theory [33,48]. The Lennard–Jones potentials, which are needed as inputs, were obtained from the CHEMKIN database. The density of the fluid was calculated using the ideal gas law. The solutions were deemed to be converged when the residuals of each of the equations decreased by seven orders of magnitude. In order to compute the actual cell voltage from the prescribed bias voltage (or potential loss), it is necessary to know the open circuit potential. As done by previous researchers [31,49], rather than use the Nernst potential, an empirical correlation [50] was used for the open circuit potential:

$$V_{OC} = 0.0025T + 0.2329 \quad (39)$$

This correlation results in an open circuit voltage of 1.04 V at 50 °C. The model was first validated (Section 3.1) against results from Jaouen et al. [15,16] prior to exercising it to study the effect of the various structural and compositional parameters of the cathode catalyst layer on fuel cell performance. The effects of cathode composition and cathode structure are presented separately in Sections 3.2 and 3.3. Baseline values for cathode model parameters and properties are listed in Table 2.

Table 1
Simulation parameters and values of key properties at 323 K and 1/1 atm

Model parameter	Value/method of calculation
Gas channel length	0.07112 m
Gas channel width	7.62×10^{-4} m
Diffusion layer width	2.54×10^{-4} m
Membrane width	1.75×10^{-4} m
Membrane permeability	1.8×10^{-18} m^2
Diffuser and catalyst layer permeability	1.76×10^{-11} m^2
Membrane porosity	0.28
Anode and cathode diffuser layer porosity	0.5
Tortuosity for Bruggemann correlation	1.5
Air side/fuel side pressures	1/1 atm
Relative humidity of inlet streams	100%
Air side inlet N_2/O_2 molar ratio	79/21
H_2 stoichiometric flow	2.8 A cm^{-2} equiv.
O_2 stoichiometric flow	3.0 A cm^{-2} equiv.
Transfer coefficients at anode (Tafel constants)	0.5
Concentration dependence at anode	0.5 (H_2)
Reference current density at anode	1.6×10^{11} (A m^{-3}) (m^3 kmol H_2)$^{-1/2}$
Membrane electrical conductivity	Springer et al. [1]
Diffuser layer electrical conductivity	100 (1 S m^{-1})

Table 2
Values of cathode model parameters and properties for baseline case

Model parameter	Value/method of calculation
Cathode Layer thickness	15 μm
Agglomerate radius	1000 nm
Polymer coating thickness	80 nm
Polymer volumetric fraction in agglomerate nucleus	0.4
Platinum mass loading	0.4 mg cm^{-2}
Platinum–carbon ratio in catalyst layer ink	0.28
Transfer coefficient at cathode (Tafel constant)	1 (≥0.8 V) [18]
	0.55 (<0.8 V) [18]
Reference exchange current density at cathode	1.288×10^{-4} A cm^{-2} (≥0.8 V) [18]
	2.291×10^{-2} A cm^{-2} (<0.8 V) [18]
Diffusion coefficient of O_2 in Nafion	3.966×10^{-10} m^2 s^{-1} [18]
Henry's constant	10 [18]

3.1. Model validation

The cathode model described in Section 2.1 was incorporated into the CFD model, described in Section 2.2, developed for predicting the PEMFC performance. A two-stage validation study was performed, in which the polarization curves were obtained for conditions described in Jaouen et al. for a theoretical baseline case [15] and a given experimental case [16]. In the first stage, the performance of the cathode catalyst model was compared with the baseline case described in Table 1 of Ref. [15] while minimizing the mass transport losses in the gas diffusion layers, Ohmic losses in the membrane, and activation and mass transport losses in the anode. In this case, the model was run for a fuel cell operating at 50 °C with H_2/O_2 gas streams at 1 atm with 70% relative humidity in the anode and cathode channels. The cathode catalyst layer was assumed to be $L = 10$ μm thick with an agglomerate radius of $r_{agg} = 0.5$ μm, a polymer coating thickness of $\delta = 0$ μm, and a polymer volumetric fraction of $\varepsilon_{agg} = 0.3$. The porosity of the cathode catalyst layer was assumed to be $\varepsilon_{cat} = 0.3$. Other details of the model are described in Table 1 of Ref. [15]. Fig. 6(a) shows the comparison between the performance predicted by the present model and the performance predicted by Jaouen et al. The double Tafel slope predicted by Jaouen et al. [15] is reproduced in the present model, and the difference between the current densities predicted by the two models is insignificant.

In the second stage of the validation test, the model developed was compared against experimental results provided in Fig. 7 of Ref. [16] for Cathode C. In this case, the model was run for a fuel cell operating at 50 °C with H_2/O_2 gas streams at 1 atm with 86% relative humidity in the anode and cathode channels. Dimensions for Cathode C with a thickness of $L = 4.7$ μm, as described in Ref. [16], were used, with an agglomerate radius of $r_{agg} = 0.11$ μm, a polymer coating thickness of $\delta = 0$ μm, and a polymer volumetric fraction

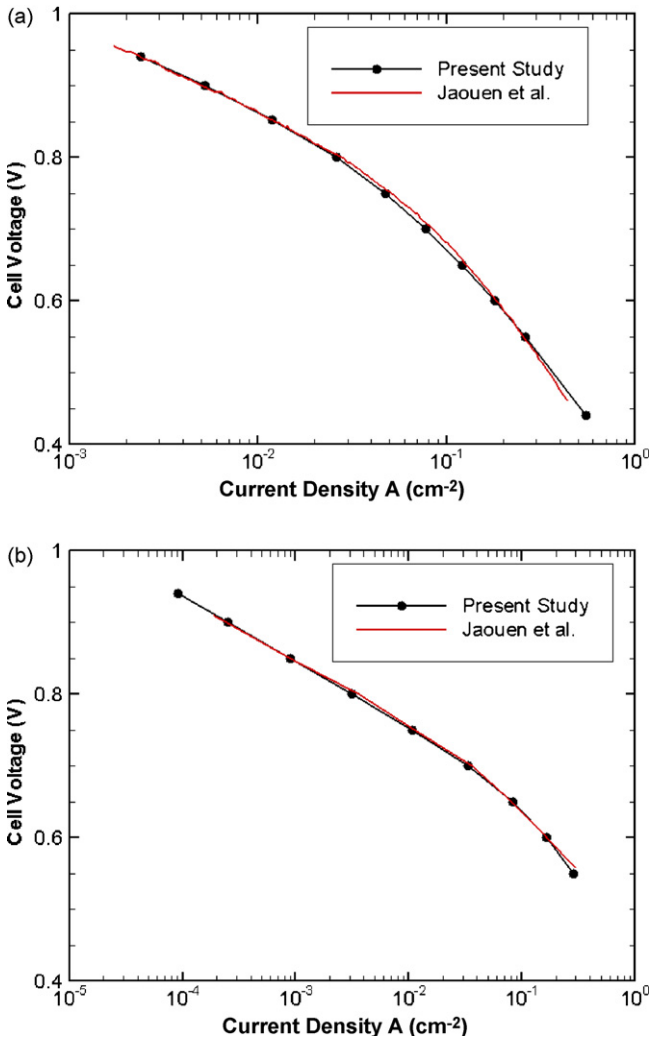

Fig. 6. Model Validation Studies: (a) comparison with model baseline case from Table 1 of Jaouen et al. [15] and (b) comparison with experimental results for "Cathode C" from Fig. 7 of Jaouen et al. [16].

of $\varepsilon_{agg} = 0.38$. The porosity of the cathode was $\varepsilon_{cat} = 0.27$. Other details regarding the parameters used in the model are available in Ref. [16]. Fig. 6(b) shows the comparison between the fuel cell performance predicted by the current model and the polarization curve obtained from the experiment. Once again, the double Tafel slope from model prediction was found to occur around the same current density and cell voltage as those measured. The results of this two-stage validation study indicate that the model developed in the present study can be used with confidence to study the effect of cathode composition and structure on fuel cell performance.

3.2. Effect of cathode composition

Following the model validation study, the effect of cathode composition on fuel cell performance was studied. To this purpose, the following four parameters were varied independently while holding the others constant:

(1) polymer (Nafion) coating thickness around agglomerate nucleus, δ;
(2) volumetric fraction of polymer (Nafion) in the agglomerate nucleus, ε_{agg};
(3) platinum mass loading, m_{Pt};
(4) platinum–carbon mass ratio in catalyst layer ink, Pt|C.

In these studies, the cathode layer thickness was held constant at $L = 15\,\mu m$ and the agglomerate radius was held constant at $r_{agg} = 1000$ nm. Other baseline values for the various parameters used in the study are presented in Table 2. As the effect of each parameter is analyzed, the optimum value for that parameter is used in subsequent studies, unless otherwise stated.

When the ionomer (Nafion) loading is changed, it can result in simultaneous change in the volume fraction of Nafion within the agglomerate (ε_{agg}) and the ionomer coating thickness (δ). However, since there are infinite many combinations of the two model parameters than can result in a certain prescribed Nafion loading value, the problem has been posed in the reverse manner, in which ε_{agg} and δ are varied independently.

3.2.1. Effect of polymer coating thickness

Fig. 7(a) shows the polarization curves for $L = 15\,\mu m$, $r_{agg} = 1000$ nm, $\varepsilon_{agg} = 0.4$, $m_{Pt} = 0.4$ mg cm^{-2}, and Pt|C = 0.28 with the polymer coating thickness (δ) varying from 0 to 100 nm. The variation of the three volume fractions, namely the volume fraction of the solid (carbon and platinum), the volume fraction of the ionomer (Nafion), and the volume fraction of the gas pores, is

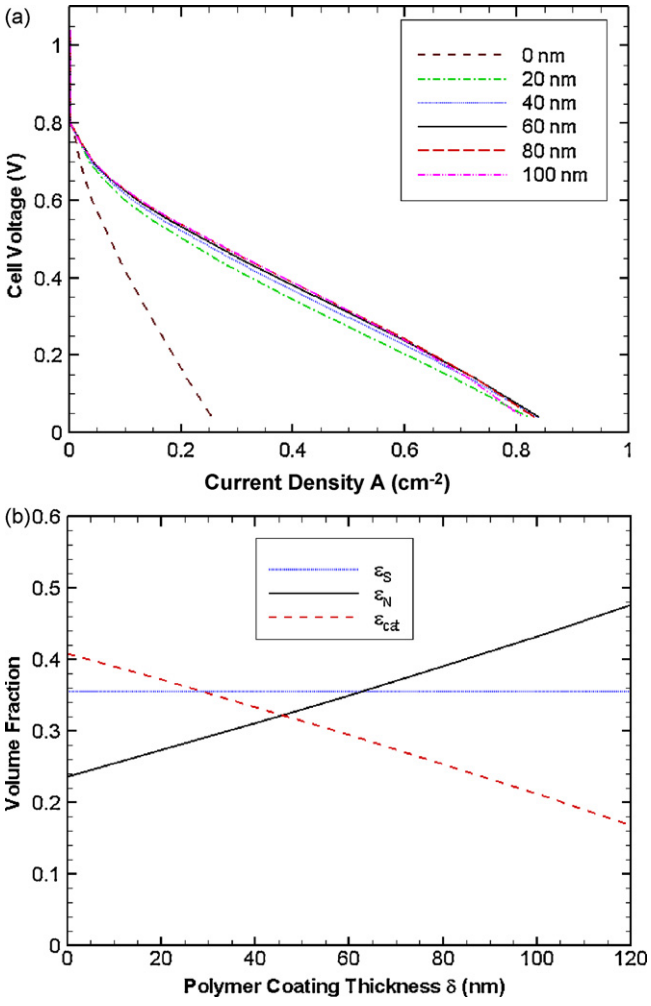

Fig. 7. Effect of polymer coating thickness (δ) on fuel cell performance for $L = 15\,\mu m$, $r_{agg} = 1000$ nm, $\varepsilon_{agg} = 0.4$, $m_{Pt} = 0.4$ mg cm^{-2}, Pt|C = 0.28. (a) Polarization curves and (b) volume fractions of platinum–carbon, Nafion and porosity.

shown separately in Fig. 7(b). It is clear from the figure that the performance of the fuel cell is poor when the coating thickness is zero. As discussed earlier, the absence of a coating indicates minimal or no contact between agglomerates, and results in few continuous paths within the catalyst layer for the protons to migrate. Thus, the protonic conductivity of the cathode catalyst layer is very small (Eq. (37) and Fig. 5) if $\delta = 0$. At the other end of the spectrum, if the coating thickness is too large, the volume fraction of Nafion within the catalyst layer (ε_{agg}) is substantial (Fig. 7(b)), and the porosity ε_{cat} is low. This results in increased mass transport losses at the catalyst layer scale (*i.e.*, global mass transport losses), as indicated by the downward bend of the polarization curve for $\delta = 100$ nm at high current densities. An optimum coating thickness is observed at higher current densities, while the optimum thickness is not as discernible at intermediate current densities, indicating that local mass transport limitations due to increased coating thickness is negligible. This observation is also consistent with Fig. 3(d), which showed earlier that the film effectiveness factor, Eff_2, is almost unity irrespective of the film coating thickness. Based on these findings, an optimum value of $\delta = 60$ nm is used in all subsequent studies.

3.2.2. Effect of polymer volume fraction in agglomerate nucleus

Fig. 8(a) shows the polarization curves for $L = 15\,\mu m$, $r_{agg} = 1000$ nm, $\delta = 60$ nm, $m_{Pt} = 0.4$ mg cm^{-2}, and Pt|C = 0.28 with the polymer (Nafion) volumetric fraction in the agglomerate nucleus (ε_{agg}) varying from 0.2 to 0.5. The variation of the three volume fractions, namely the volume fraction of the solid (carbon and platinum), the volume fraction of the ionomer (Nafion), and the volume fraction of the gas pores, is shown separately in Fig. 8(b). The polarization curves show that at low to medium current densities, the performance of the fuel cell improves with increasing values of ε_{agg}. This is due to the fact that the polymer content in the cathode increases as ε_{agg} increases, thereby reducing the mass transport resistance within the agglomerate nucleus (Eq. (4) and Fig. 3(a)–(c)). At medium current densities, there is no clear optimal performance for varying polymer volumetric fraction within the agglomerate nucleus, indicating that at the local or agglomerate-scale, increasing the amount of Nafion within the agglomerate is always beneficial. These results also imply that experimentally observed optimum performance with varying Nafion (polymer) content [3,5] in a cathode is due to variation in the polymer coating thickness rather than due to the variation of the polymer volumetric fraction within the agglomerate nucleus. At high current densities, however, global mass transport losses increase due to decrease in the porosity (ε_{cat}) of the cathode catalyst layer, as shown in Fig. 8(b). Based on the results of this study, an optimal value of $\varepsilon_{agg} = 0.4$ is used in all subsequent studies. It is worth mentioning at this point that the optimum values chosen for δ (preceding sub-section) and ε_{agg}, *i.e.*, $\delta = 60$ nm, and $\varepsilon_{agg} = 0.4$, both yield overall catalyst layer porosity values, ε_{cat}, of approximately 0.28, as seen in Figs. 7(b) and 8(b). Incidentally, a value of 0.28 has been widely cited in past studies, both experimental and numerical [30,31,46,47,49].

3.2.3. Effect of platinum mass loading

Fig. 9(a) shows the polarization curves for L = 15 μm, $r_{agg} = 1000$ nm, $\delta = 60$ nm, $\varepsilon_{agg} = 0.4$, and Pt|C = 0.28 with platinum mass loading (m_{Pt}) varying from 0.2 to 0.5 mg cm^{-2}. The platinum mass loading is defined as the mass of platinum used per unit area of the bi-polar plate through which the current is collected. The variation of the three volume fractions, namely ε_{cat}, ε_N, and ε_S is shown separately in Fig. 9(b). At low to intermediate current densities, increase in platinum mass loading results in better performance, as is evident from Fig. 9(a). This

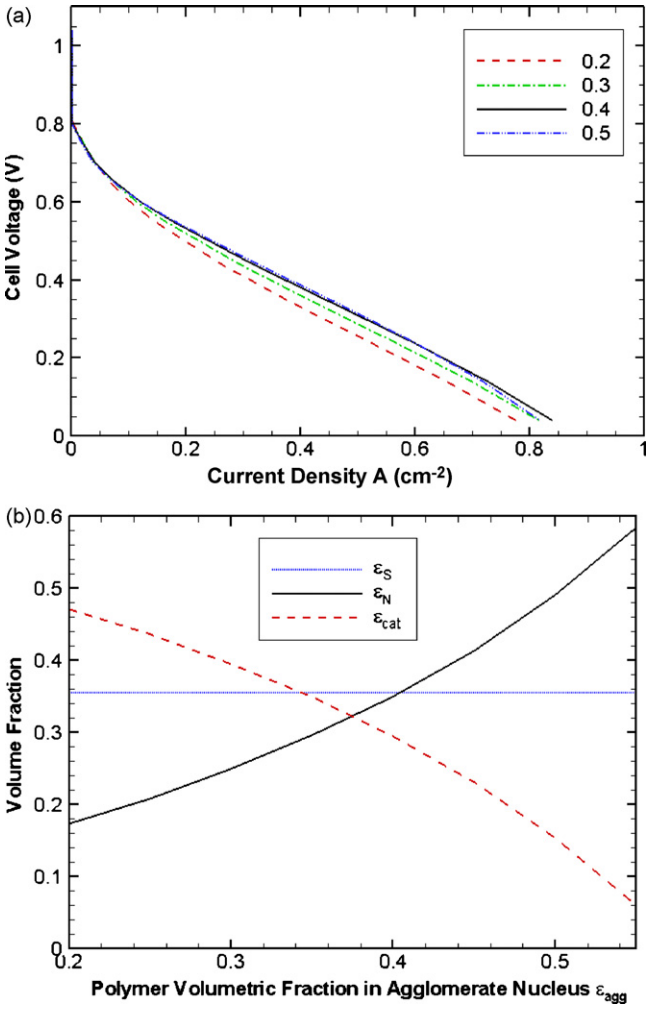

Fig. 8. Effect of polymer volumetric fraction in agglomerate nucleus (ε_{agg}) on fuel cell performance for $L = 15\,\mu m$, $r_{agg} = 1000$ nm, $\delta = 60$ nm, $m_{Pt} = 0.4$ mg cm^{-2}, Pt|C = 0.28. (a) Polarization curves and (b) volume fractions of platinum–carbon, Nafion and porosity.

is due to the fact that, at high platinum loading, the amount of catalyst surface available for the oxygen reduction reaction to take place is high (Eq. (9)). At high current densities, however, global mass transport effects begin to influence fuel cell performance. This is due to the sharp decrease in cathode porosity, ε_{cat}, with increasing platinum loading, as shown in Fig. 9(b), which in turn results in increased mass transport resistance at the cathode catalyst layer scale. Thus, aside of cost considerations, there is a valid physics-based reason not to use excessive amounts of platinum in PEMFC cathodes. Based on the results of this study, an optimum value of $m_{Pt} = 0.45$ mg cm^{-2} is used in all subsequent studies.

3.2.4. Effect of platinum–carbon mass ratio

Fig. 10(a) shows the polarization curves for $L = 15\,\mu m$, $r_{agg} = 1000$ nm, $\delta = 60$ nm, $\varepsilon_{agg} = 0.4$, and $m_{Pt} = 0.45$ mg cm^{-2} with platinum–carbon mass ratio (Pt|C) varying from 0.25 to 0.4. Changing the Pt|C ratio with a fixed platinum mass loading implies that the amount of carbon within the agglomerates is changed. Furthermore, since the volume fraction of Nafion within the agglomerate, ε_{agg}, is also to be kept unchanged, change in the amount of carbon must also be accompanied by a changing in the amount of Nafion within the catalyst layer. The variation of the three relevant

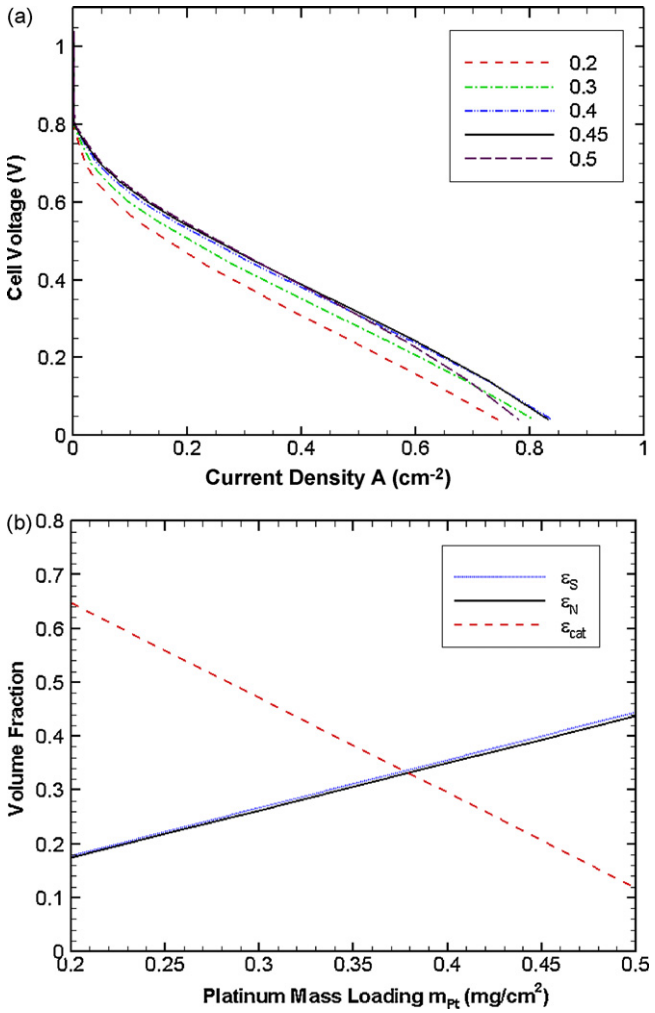

Fig. 9. Effect of platinum mass loading (m_{Pt}) on fuel cell performance for $L = 15\ \mu m$, $r_{agg} = 1000$ nm, $\delta = 60$ nm, $\varepsilon_{agg} = 0.4$, Pt|C = 0.28. (a) Polarization curves and (b) volume fractions of platinum–carbon, Nafion and porosity.

global volume fractions is shown in Fig. 10(b). It can be seen that at low platinum–carbon mass ratios, the porosity of the cathode is low. Based on the above discussion, low Pt|C ratio implies large amounts of carbon, which also implies large amounts of Nafion. Thus, low Pt|C ratio produces poor performance due to increased mass transport resistance to diffusion of gases through the pores, as indicated by the strong bending of the dotted red curve at high current densities. At the other end, excessively high values of Pt|Cratio imply that there is too little Nafion within the cathode, thereby reducing the protonic conductivity of the cathode. Thus, we see that higher Pt|C values give rise to lower performance, irrespective of the current density. Based on the results of the current study, an optimum value of Pt|C = 0.28 is used in all subsequent studies.

3.3. Effect of cathode structure

In order to study the effect of cathode structure on fuel cell performance, the following two parameters were varied independently:

(1) agglomerate radius (r_{agg});
(2) cathode layer thickness (L).

3.3.1. Effect of agglomerate radius

Fig. 11(a) shows the polarization curves for $L = 15\ \mu m$, $\delta = 60$ nm, $\varepsilon_{agg} = 0.4$, $m_{Pt} = 0.45\ mg\ cm^{-2}$, and Pt|C = 0.28 with agglomerate radius (r_{agg}) varying from 600 to 1200 nm. In this first study, the coating thickness is kept unchanged even though the agglomerate radius is changed. This implies, that the volume fraction of Nafion within the catalyst layer, ε_N, will change, as will the overall porosity of the cathode catalyst layer. The variation of the three relevant global volume fractions is shown in Fig. 11(b). Fig. 11(a) shows that as the agglomerate radius increases, the performance of the fuel cell deteriorates. Essentially, smaller agglomerates pose smaller resistance to mass transport at the agglomerate (local) scale, as was also illustrated in Fig. 3(a)–(c). Thus, the performance monotonically improves with decrease in agglomerate radius, as predicted by Sun et al. [18] and Secanell et al. [19]. However, experimental results [27] suggest that performance deteriorates if the agglomerate size is too small. Some authors [15,16,27] cite this as Knudsen effects. They argue that small agglomerate sizes also result in very small pores, within which Knudsen effects are manifested. However, since ballistic transport poses lower resistance than diffusive transport, it is not clear if Knudsen effects can account for this deterioration in performance, *i.e.*, increase in mass transport resistance. It is our contention that this deterioration of performance for

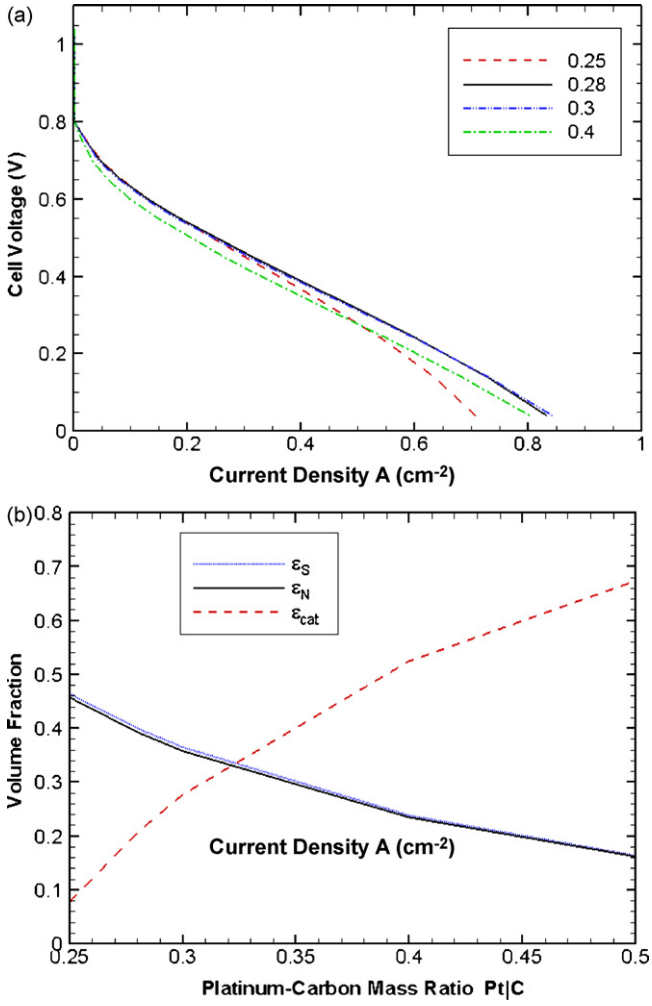

Fig. 10. Effect of platinum–carbon mass ratio in catalyst layer ink (Pt|C) on fuel cell performance for $L = 15\ \mu m$, $r_{agg} = 1000$ nm, $\delta = 60$ nm, $\varepsilon_{agg} = 0.4$, $m_{Pt} = 0.45\ mg\ cm^{-2}$. (a) Polarization curves and (b) volume fractions of platinum–carbon, Nafion and porosity.

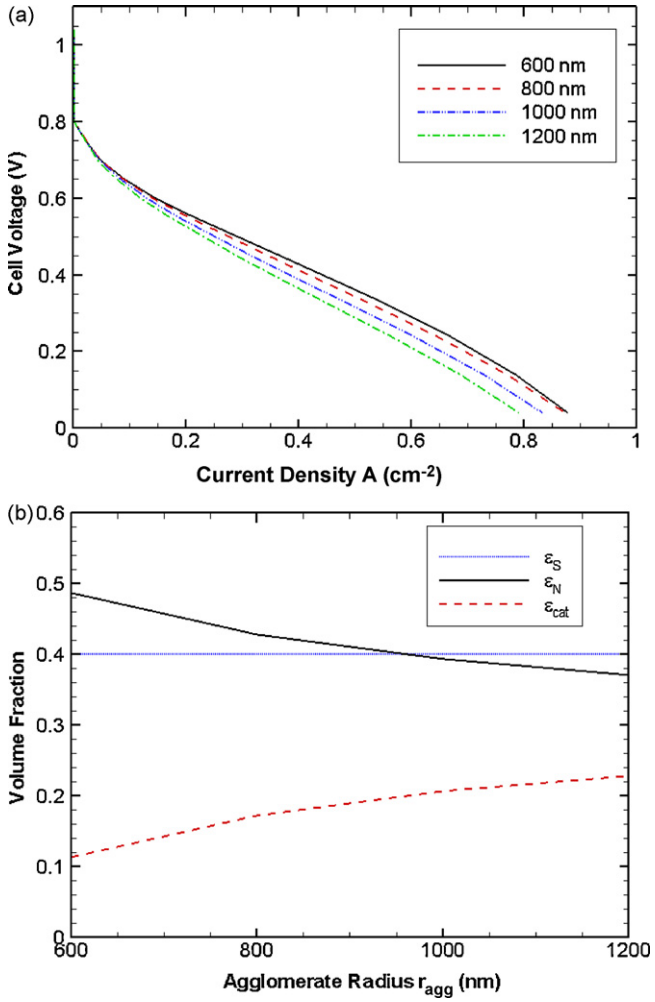

Fig. 11. Effect of agglomerate radius (r_{agg}) on fuel cell performance for $L = 15\,\mu m$, $\delta = 60\,nm$, $\varepsilon_{agg} = 0.4$, $m_{Pt} = 0.45\,mg\,cm^{-2}$, Pt|C = 0.28. (a) Polarization curves and (b) volume fractions of platinum–carbon, Nafion and porosity.

small agglomerate sizes is due to increased tortuosity of the pores. Experimental and theoretical studies [28] clearly indicate that a box packed randomly with large rigid spheres pose smaller resistance to diffusion than a box packed with small spheres with the same overall porosity. The model used here (Eq. (23) and Fig. 4) clearly captures this physics. As a result, our model predictions indeed show (Fig. 11(a)) that at high current densities, smaller sizes do not result in improved performance. The optimum is governed by the balance between decreased local mass transport resistance due to smaller agglomerate size and an increased global mass transport resistance due to increased tortuosity.

In the first set of studies, just described, change in the agglomerate radius also resulted in change of the three relevant global volume fractions. In other words, the structural parameter affected the compositional parameters. In order to isolate the effect of the structural parameter on fuel cell performance, agglomerate radius needs to be varied in such a way that the volume fractions of platinum–carbon, Nafion and the porosity of the cathode remain constant. This is achieved by varying the agglomerate radius while keeping the ratio between polymer coating thickness and the agglomerate radius constant (see Fig. 12(b)). Fig. 12(a) shows the polarization curves for $L = 15\,\mu m$, $\delta/r_{agg} = 0.06$, $\varepsilon_{agg} = 0.4$, $m_{Pt} = 0.45\,mg\,cm^{-2}$, and Pt|C = 0.28 with agglomerate radius (r_{agg}) varying from 50 nm to 1000 nm. From Fig. 12(a), it is clear that while performance improves with decreasing agglomerate radius, at very low values of r_{agg}, there is no significant change in performance, as explained in the preceding paragraph. In fact, at high current densities, the performance for $r_{agg} = 100\,nm$ is seen to be marginally better than that for $r_{agg} = 50\,nm$. This implies that cathode tortuosity has a significant influence on fuel cell performance at low values of agglomerate radius.

3.3.2. Effect of cathode catalyst layer thickness

Fig. 13(a) shows the polarization curves for $r_{agg} = 200\,nm$, $\delta/r_{agg} = 0.06$, $\varepsilon_{agg} = 0.4$, and Pt|C = 0.28 for cathode layer thicknesses of $L = 7.5$, 15, and 30 μm. The cathode catalyst layer thickness is a global structural parameter, and it does not affect the three relevant porosities, as is clear from Fig. 13(b). It can be seen that the performance is superior for $L = 15\,\mu m$ compared to the $L = 7.5\,\mu m$ case. This is due to the fact that the reactant gases do not have as many reaction sites in the latter case as in the former case. Comparing $L = 15$ and 30 μm, it can be seen that the latter thickness provides better performance at low and intermediate current densities. Due to increased mass transport resistance for $L = 30\,\mu m$, at higher current densities, the reactant gases are unable to reach all the reaction sites, and the catalyst at the inner half of the catalyst layer (*i.e.*, adjacent to the membrane) largely remain underutilized.

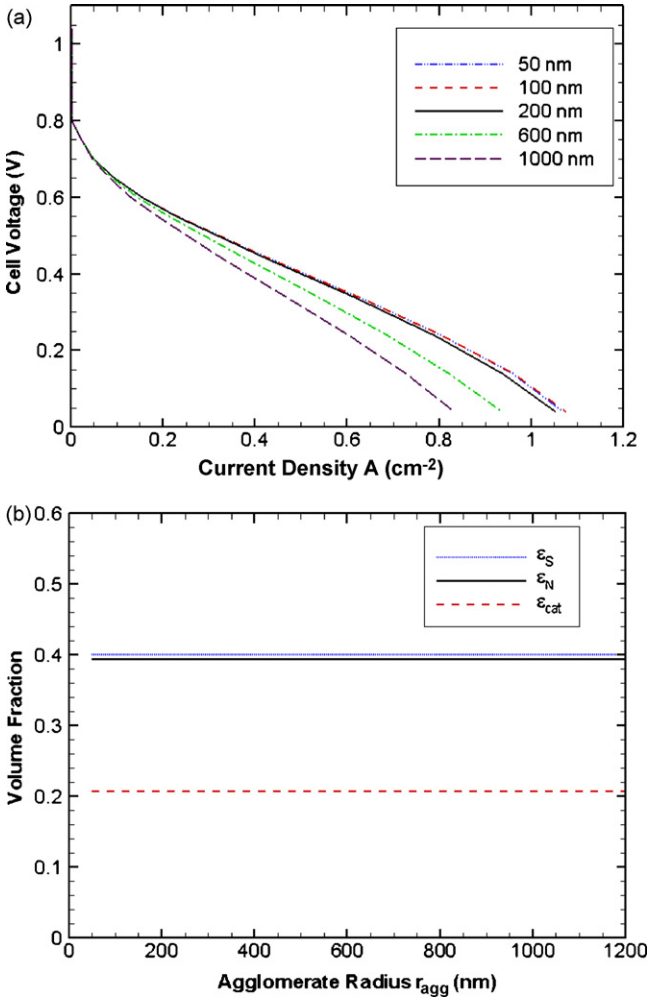

Fig. 12. Effect of agglomerate radius (r_{agg}) on fuel cell performance for $L = 15\,\mu m$, $\delta/r_{agg} = 0.06$, $\varepsilon_{agg} = 0.4$, $m_{Pt} = 0.45\,mg\,cm^{-2}$, Pt|C = 0.28. (a) Polarization curves and (b) volume fractions of platinum–carbon, Nafion and porosity.

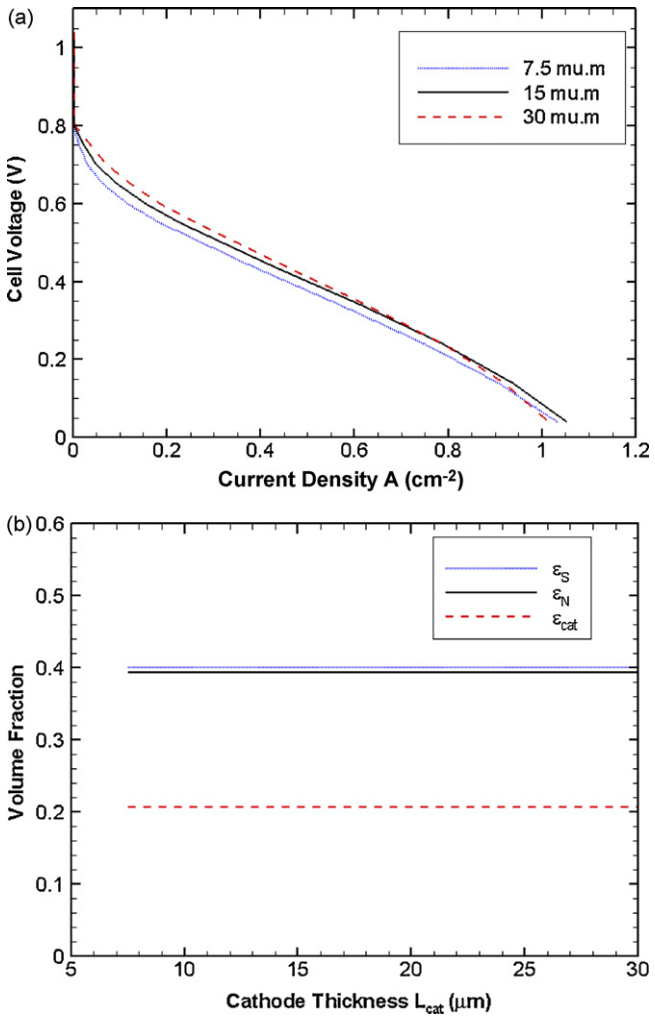

Fig. 13. Effect of cathode catalyst layer thickness (L) on fuel cell performance for r_{agg} = 200 nm, δ/r_{agg} = 0.06, ε_{agg} = 0.4, Pt|C = 0.28. (a) Polarization curves and (b) volume fractions of platinum–carbon, Nafion and porosity.

4. Summary and conclusions

With the advent of next-generation techniques for micro-/nano-fabrication, it will be possible to engineer fuel cell catalyst layers (electrodes) to desired compositions and structures. If a model is available that is general enough to answer the question, even qualitatively, as to what structure and composition is best for optimum performance, its impact on the advancement of fuel cell technology could be unprecedented. The model developed in this study fulfills this critical need. The sub-grid scale cathode catalyst model, based on the flooded agglomerate concept, was first validated against previously published experimental data. Following the validation phase, the effects of Nafion loading, platinum loading, platinum–carbon ratio, agglomerate size and cathode layer thickness on the performance of a polymer electrolyte membrane fuel cell were studied. Based on these studies, the following conclusions may be drawn:

(1) Variation of engineering parameters such as platinum loading or Nafion loading leads to simultaneous change in several of the model parameters—most notably the volume fractions of the pores, Nafion and solid. Thus, the performance of the overall fuel cell is a manifestation of a complex interaction of several model parameters.

(2) The effect of each parameter on the overall performance of a fuel cell is different at different operating points (current densities). While local (or agglomerate-scale) mass transport effects can be understood simply by carefully studying the effectiveness factors shown in Fig. 3, global mass transport losses require incorporation of the sub-grid scale catalyst layer model into full-scale CFD calculations.

(3) At medium current densities, variation of compositional parameters usually affects performance due to local mass transport and electrical conduction limitations, while at high current densities, performance is primarily affected due to global mass transport limitations introduced arising from varying porosity.

(4) The presence of an optimal performance with varying Nafion content in the cathode is more due to the local agglomerate-level mass transport and conductivity losses in the polymer coating around the agglomerates than due to the amount of Nafion within the agglomerate.

(5) In addition to cost constraints, platinum mass loading needs to be at a moderate level in order to optimize fuel cell performance.

(6) Cathode tortuosity has a significant effect on fuel cell performance at low values of agglomerate radius. Thus, it is not desirable to design cathodes in which the carbon particle sizes (or pore sizes) are too small. While this may result in reduced agglomerate-scale mass transport losses, it is undesirable due to poor diffusion of reactants through the pores.

In the future, the study will be extended to include the effect of liquid water. However, the authors hope that this study has been able to lay a solid foundation for further advancement in this area.

References

[1] R. O'Hayre, D. Barnett, F. Prinz, J. Electrochem. Soc. 152 (2) (2005) A439–A444.
[2] M. Zhu, X.-Z. Xu, R. Su, J.-M. Yang, J. Electrochem. Soc. 152 (3) (2005) A511–A515.
[3] G. Sasikumar, J. Ihm, H. Ryu, J. Power Sources 132 (2004) 11–17.
[4] Z. Xie, T. Navessin, K. Shi, R. Chow, Q. Wang, D. Song, B. Andreaus, M. Eikerling, Z. Liu, S. Holdcroft, J. Electrochem. Soc. 152 (6) (2005) A1171–A1179.
[5] D. Song, Q. Wang, Z. Liu, T. Navessin, M. Eikerling, S. Holdcroft, J. Power Sources 126 (2004) 104–111.
[6] C. Marr, X. Li, J. Power Sources 77 (1999) 17–27.
[7] A. Kulikovsky, J. Divisek, A. Kornyshev, J. Electrochem. Soc. 146 (11) (1999) 3981–3991.
[8] M. Secanell, B. Carnes, A. Suleman, N. Djilali, Electrochim. Acta 52 (7) (2007) 2668–2682.
[9] D.H. Schwarz, N. Djilali, J. Electrochem. Soc. 154 (11) (2007) B1167–B1178.
[10] T. Springer, I. Raistrick, J. Electrochem. Soc. 136 (6) (1989) 1594.
[11] S.J. Ridge, R.E. White, Y. Tsou, R.N. Beaver, G.A. Eisman, J. Electrochem. Soc. 136 (7) (1989) 1902–1909.
[12] M.L. Perry, J. Newman, E.J. Cairns, J. Electrochem. Soc. 145 (1) (1998) 5–15.
[13] P.-C. Sui, L.-D. Chen, J. Seaba, Y. Wariishi, SAE Technical Paper, Number 1999-01-0539, 1999.
[14] M. Eikerling, A. Kornyshev, J. Electroanal. Chem. 475 (1999) 107–123.
[15] F. Jaouen, G. Lindbergh, G. Sundholm, J. Electrochem. Soc. 149 (4) (2002) A437–A447.
[16] F. Jaouen, G. Lindbergh, K. Wiezell, J. Electrochem. Soc. 150 (12) (2003) A1711–A1717.
[17] L. Pisani, M. Valentini, G. Murgia, J. Electrochem. Soc. 150 (12) (2003) A1549–A1559.
[18] W. Sun, B.A. Peppley, K. Karan, Electrochim. Acta 50 (2005) 3359–3374.
[19] M. Secanell, K. Karan, A. Suleman, N. Djilali, Electrochim. Acta 52 (22) (2007) 6318–6337.
[20] N. Siegel, M. Ellis, D. Nelson, M. Von Spakovsky, J. Power Sources 128 (2004) 173–184.
[21] H. Gasteiger, J. Panels, S. Yan, J. Power Sources 127 (2004) 162–171.
[22] K. Jeng, C. Kuo, S. Lee, J. Power Sources 128 (2004) 145–151.
[23] Z. Farhat, J. Power Sources 138 (2005) 68–78.
[24] K.-M. Yin, J. Electrochem. Soc. 152 (3) (2005) A583–A593.
[25] G. Wang, P.P. Mukherjee, C.-Y. Wang, Electrochim. Acta 51 (2006) 3139–3150.
[26] P.P. Mukherjee, C.-Y. Wang, J. Electrochem. Soc. 153 (5) (2006) A840–A849.
[27] Jaouen, F., Electrochemical Characterization of Porous Cathodes in the Polymer Electrolyte Fuel Cell, Ph.D. Thesis, Kungl Tekniska Hogskolan, Stockholm, 2003.
[28] M. Kaviany, Principles of Heat Transfer in Porous Media, Springer-Verlag, 1991.
[29] S. Kamarajugadda, S. Mazumder, Comput. Chem. Eng. 32 (7) (2008) 1650–1660.

[30] S. Dutta, S. Shimpalee, J.W. Van Zee, Int. J. Heat Mass Transf. 44 (11) (2001) 2029–2042.
[31] S. Mazumder, J.V. Cole, J. Electrochem. Soc. 150 (11) (2003) A1503–A1509.
[32] S. Mazumder, J.V. Cole, J. Electrochem. Soc. 150 (11) (2003) A1510–A1517.
[33] R.B. Bird, W. Stewart, E.N. Lightfoot, Transport Phenomena, 2nd ed., Wiley, New York, 2001.
[34] M.H. Abbasi, J.W. Evans, I.S. Abramson, AIChE J. 29 (4) (1983) 617–624.
[35] D.G. Huizenga, D.M. Smith, AIChE J. 32 (1) (1986) 1–6.
[36] J.S. Newman, Electrochemical Systems, Prentice-Hall, New York, 1973.
[37] G. Janssen, J. Electrochem. Soc. 148 (12) (2001) A1313–A1323.
[38] A. Weber, J. Newman, J. Electrochem. Soc. 150 (7) (2003) A1008–A1015.
[39] A. Weber, J. Newman, J. Electrochem. Soc. 151 (2) (2004) A311–A325.
[40] A. Weber, J. Newman, J. Electrochem. Soc. 151 (2) (2004) A326–A339.
[41] T. Thampan, S. Malhotra, H. Tang, R. Datta, J. Electrochem. Soc. 147 (9) (2000) 3242–3250.
[42] S. Mazumder, J. Electrochem. Soc. 152 (8) (2005) A1633–A1644.
[43] T. Fuller, J. Newman, J. Electrochem. Soc. 140 (5) (1993) 1211–1225.
[44] T.E. Springer, T.A. Zawodzinski, S. Gottesfeld, J. Electrochem. Soc. 138 (8) (1991) 2334–2342.
[45] S.V. Patankar, Numerical Heat Transfer and Fluid Flow, Hemisphere Publishing Corporation, Washington, DC, 1980.
[46] E.A. Ticianelli, C.R. Derouin, S. Srinivasan, J. Electroanal. Chem. 251 (2) (1988) 275–295.
[47] E.A. Ticianelli, C.R. Derouin, A. Redondo, S. Srinivasan, J. Electrochem. Soc. 135 (9) (1988) 2209–2214.
[48] J.O. Hirschfelder, C.F. Curtiss, R.B. Bird, Molecular Theory of Gases and Liquids, Wiley, New York, 1954.
[49] V. Gurau, H. Liu, S. Kakac, AIChE J. 44 (11) (1998) 2410–2422.
[50] A. Parthasarathy, S. Srinivasan, A.J. Appleby, J. Electrochem. Soc. 139 (9) (1992) 2530–2537.